JACS
JOURNAL OF THE AMERICAN CHEMICAL SOCIETY

ARTICLE

pubs.acs.org/JACS

Synthesis of Pd−Pt Bimetallic Nanocrystals with a Concave Structure through a Bromide-Induced Galvanic Replacement Reaction

Hui Zhang,[II,†,‡] Mingshang Jin,[II,†,§] Jinguo Wang,[⊥] Weiyang Li,[†] Pedro H. C. Camargo,[†] Moon J. Kim,[⊥] Deren Yang,[‡] Zhaoxiong Xie,[§] and Younan Xia*[,†]

[†]Department of Biomedical Engineering, Washington University, St. Louis, Missouri 63130, United States

[‡]State Key Laboratory of Silicon Materials and Department of Materials Science and Engineering, Zhejiang University, Hangzhou, Zhejiang 310027, People's Republic of China

[§]State Key Laboratory for Physical Chemistry of Solid Surfaces and Department of Chemistry, College of Chemistry and Chemical Engineering, Xiamen University, Xiamen, Fujian 361005, People's Republic of China

[⊥]Department of Materials Science, University of Texas at Dallas, Richardson, Texas 75083, United States

Supporting Information

ABSTRACT: This article describes a systematic study of the galvanic replacement reaction between $PtCl_6^{2-}$ ions and Pd nanocrystals with different shapes, including cubes, cuboctahedrons, and octahedrons. It was found that Br^- ions played an important role in initiating, facilitating, and directing the replacement reaction. The presence of Br^- ions led to the selective initiation of galvanic replacement from the {100} facets of Pd nanocrystals, likely due to the preferential adsorption of Br^- ions on this crystallographic plane. The site-selective galvanic replacement resulted in the formation of Pd−Pt bimetallic nanocrystals with a concave structure owing to simultaneous dissolution of Pd atoms from the {100} facets and deposition of the resultant Pt atoms on the {111} facets. The Pd−Pt concave nanocubes with different weight percentages of Pt at 3.4, 10.4, 19.9, and 34.4 were also evaluated as electrocatalysts for the oxygen reduction reaction (ORR). Significantly, the sample with a 3.4 wt.% of Pt exhibited the largest specific electrochemical surface area and was found to be four times as active as the commercial Pt/C catalyst for the ORR in terms of equivalent Pt mass.

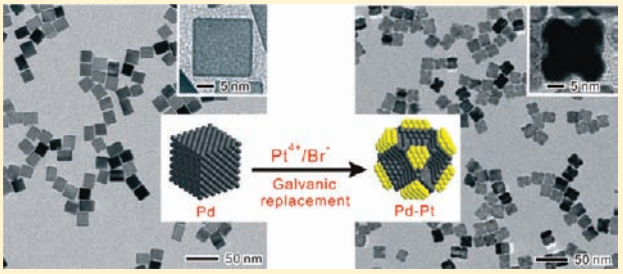

INTRODUCTION

Noble-metal nanocrystals with a concave structure on the surface have physical/chemical properties different from those enclosed by a flat or convex surface.[1−5] Owing to their unusual facets and negative curvature, nanocrystals with a concave structure have also received attention for a number of applications related to catalysis, electrocatalysis, optical sensing, and localized surface plasmon resonance.[6−8] In general, overgrowth and etching represent two powerful routes to the synthesis of nanocrystals with a concave structure. For overgrowth, the formation of a concave structure is typically achieved under kinetic control to overcome the requirement of minimizing the total surface free energy. In comparison, the formation of a concave structure by etching has to rely on an anisotropic process, in which a specific set of facets of the template are preferentially dissolved over others. Compared to the remarkable success in the synthesis of nanocrystals enclosed by a flat or convex surface (with examples including cube, octahedron, tetrahedron, decahedron, icosahedron, plate, bar, and rod),[9−11] there are only a few reports on the synthesis of metal nanocrystals with a concave structure. To this end, we have demonstrated the synthesis Pt tetrahedra and octahedra with concave facets using an overgrowth approach.[12] We have demonstrated the syntheses of Au nanocages and nanoframes with cavities on the surfaces using a galvanic replacement reaction between Ag nanocrystals and a Au(I) or Au(III) salt precursor.[13] We have also demonstrated the synthesis of Pd nanocages using an oxidative etching process.[14] Zheng and co-workers reported the synthesis of tetrahedral and trigonal bipyramidal nanoframes of Pd using a solvothermal process in the presence of formaldehyde.[15] Berkovitch and co-workers demonstrated a technique based on electron beam lithography (EBL) for fabricating arrays of concave hyperbolic Au particles on glass substrates with controllable concavity via an etching strategy.[16] Mirkin and co-workers demonstrated the synthesis of Au concave nanocubes via seed-mediated overgrowth with cetyltrimethylammonium chloride (CTAC) as a capping agent.[17] Most recently, we reported a facile process for the formation of Rh, Pt, and Pt/Rh concave nanocubes by manipulating the reaction kinetics with a syringe pump to alter the injection rate of a salt precursor.[18,19] It still remains a grand challenge to extend these strategies to other

Received: February 6, 2011
Published: March 25, 2011

   dx.doi.org/10.1021/ja201156s | J. Am. Chem. Soc. 2011, 133, 6078–6089

metals to generate nanocrystals with a concave structure and relatively small sizes (below 20 nm).

As a strategy based on etching, galvanic replacement represents a remarkably simple and versatile route to the synthesis of bimetallic nanostructures with hollow interiors as well as cavities and thus negative curvatures on the surface.[20−22] In a galvanic replacement reaction, the electrochemical potential difference between a sacrificial template and the metal ions in a solution drives the reaction, i.e., oxidation and dissolution of the template accompanied by reduction of ions of another metal and deposition of the resultant atoms on the surface of the template. The size and morphology of the final product can be readily manipulated by using sacrificial templates with different sizes and shapes and/or by controlling the extent of replacement. As demonstrated in our previous work, Ag nanocrystals with a variety of shapes, including nanocubes, nanospheres, nanorods, and nanowires, can all react with Au(III) or Au(I), Pt(IV) or Pt(II), and Pd(II) salt precursors to generate bimetallic nanostructures in the form of box, cage, frame, shell, rattle, and tube.[23−25] As a sacrificial template for the synthesis of bimetallic or alloyed nanostructures, Ag nanocrystals have a number of limitations: For example, their sizes are typically larger than 20 nm; the remaining Ag may cause instability and poisoning issues for a catalyst; and the remaining Ag may cause toxicity for biomedical applications. In order to avoid these limitations or potential problems, Pd nanocrystals have been recognized as an alternative candidate for the galvanic reaction due to their availability in a myriad of well-defined shapes and with sizes controllable down to a few nanometers. This is particularly useful in the synthesis of Pt-based catalysts for various applications. For the system involving Pd nanocrystals and a Pt precursor, however, no galvanic replacement seemed to occur between them under conventional conditions despite their large difference in electrochemical potential.[26] In addition, compared with the system involving Ag nanocrystals and a Au precursor, very little is known about the mechanistic details associated with the heterogeneous nucleation and growth of Pt on templates made of Pd nanocrystals during a galvanic replacement process.

Herein we report a bromide-induced galvanic replacement reaction between $PtCl_6^{2-}$ ions and Pd nanocrystals with different shapes for generating Pd−Pt bimetallic nanocrystals with a concave structure. The Pd−Pt concave nanocrystals are of particular interest and importance for catalytic or electrocatalytic applications owing to the following attractive features: (i) they can offer much higher specific surface areas and thus improved activity relative to their solid counterparts;[27,28] (ii) the presence of a cavity in the Pt layer and a Pd core in the interior can help reduce the loading of Pt, an extremely scarce and expensive noble metal;[29,30] and (iii) the use of Pd in the core instead of other metals, such as Ag or Co, eliminates the corrosion by an acidic in a proton-exchange membrane (PEM) fuel cell.[31,32] In addition, Pt nanostructures supported on Pd substrates may exhibit enhanced activity for the oxygen reduction reaction (ORR) at the cathode of a PEM fuel cell in comparison with pure Pt.[33,34] Specifically in this work, we have evaluated Pd nanocrystals with various shapes, including cubes, octahedrons, and cuboctahedrons, as templates for the galvanic replacement reaction with $PtCl_6^{2-}$ ions in an aqueous solution. The use of Pd nanocrystals with different shapes (and thus facets) as templates allowed us to systematically investigate the selectivity of facet during a galvanic replacement reaction. Using this simple approach, we have been able to routinely produce Pd−Pt bimetallic concave nanocrystals with high specific surface areas. Our electrochemical data clearly demonstrate that the Pd−Pt concave nanocubes have substantially enhanced ORR mass activity as compared to the commercial Pt/C catalyst. The ORR activity also showed a strong dependence on the compositions of the Pd−Pt bimetallic nanocrystals, with the highest activity being observed for a Pt weight percentage of 3.4.

EXPERIMENTAL SECTION

Chemicals and Materials. Sodium tetrachloropalladate (II) (Na_2PdCl_4, Sigma-Aldrich, 99.998%), hexachloroplatinic acid (H_2PtCl_6, Sigma-Aldrich, 99.995%), potassium bromide (KBr, Fisher Scientific), potassium chloride (KCl, T. J. Baker), poly(vinyl pyrrolidone) (PVP, MW ≈ 55 000, Sigma-Aldrich), ascorbic acid (AA, Sigma-Aldrich), formaldehyde (Fisher Scientific), acetone (EMD), and ethanol (Pharmco Products, 200 proof) were all used as received. All aqueous solutions were prepared using deionized water with a resistivity of 18.2 MΩ·cm. All syntheses were carried out in glass vials (20 mL, VWR international).

Synthesis of Pd Nanocubes. The Pd nanocubes were synthesized by adding a Na_2PdCl_4 solution into a mixture of AA, KBr, and KCl according to our previous report.[35] In a typical synthesis, 8.0 mL of an aqueous solution containing 105 mg of PVP, 60 mg of AA, and different amounts of KBr and KCl was hosted in a vial and preheated to 80 °C in an oil bath under magnetic stirring for 10 min. Subsequently, 3.0 mL of an aqueous solution containing 57 mg of Na_2PdCl_4 was added with a pipet. After the vial had been capped, the reaction was allowed to continue at 80 °C for 3 h. The size of Pd nanocubes was controlled by varying the amounts of KBr and KCl: For example, the use of 600 mg of KBr, 300 mg of KBr, and 5 mg of KBr together with 185 mg of KCl resulted in the formation of Pd nanocubes about 18, 10, and 6 nm in size, respectively. The product was collected by centrifugation, washed three times with water to remove excess PVP, and redispersed in 11 mL water.

Synthesis of Pd Cuboctahedrons and Octahedrons. These nanocrystals were prepared by adding 3 mL of aqueous Na_2PdCl_4 solution (9.5 mg/mL) into an aqueous solution (8 mL) containing 105 mg of PVP, 100 μL of HCHO, and different amounts of the Pd nanocubes (18 nm in size) at 60 °C under magnetic stirring. The morphology of resultant nanocrystals was determined by the amount of Pd nanocubes added as the seeds. The use of 1.0 and 0.3 mL of the suspension of Pd nanocubes resulted in the formation of cuboctahedrons of 25 nm in size and octahedrons of 33 nm in size, respectively. For each synthesis, the vial was removed from the oil bath after 3 h. After collection by centrifugation and washing three times with water, the product was redispersed in 11 mL water. For the synthesis of Pd octahedrons of 16 nm in size, the procedure was exactly the same as what we used in a previous study.[11]

Synthesis of Pd−Pt Bimetallic Nanocrystals via Galvanic Replacement. In a standard procedure, 1 mL of the aqueous suspension of Pd nanocubes (18 nm in size) and 7 mL of an aqueous solution containing PVP (33.3 mg) and KBr (300 mg) were mixed in a glass vial. The mixture was heated to 90 °C in air under magnetic stirring. Meanwhile, 3.5 mg of H_2PtCl_6 was dissolved in 3 mL deionized water. This aqueous solution was then injected into the solution containing PVP, KBr, and Pd nanocrystals using a syringe pump at a rate of 1 mL/min. The reaction mixture was then heated to 90 °C for 12 h in air. Finally, the solution was centrifuged and washed three times with water to remove PVP before characterization. We systematically investigated the effects of various parameters, including the duration of reaction, the amount of H_2PtCl_6, the shape of the Pd nanocrystals, and the temperature as well as the amounts of KBr and KCl on the morphology of resultant Pd−Pt nanocrystals.

dx.doi.org/10.1021/ja201156s |J. Am. Chem. Soc. 2011, 133, 6078–6089

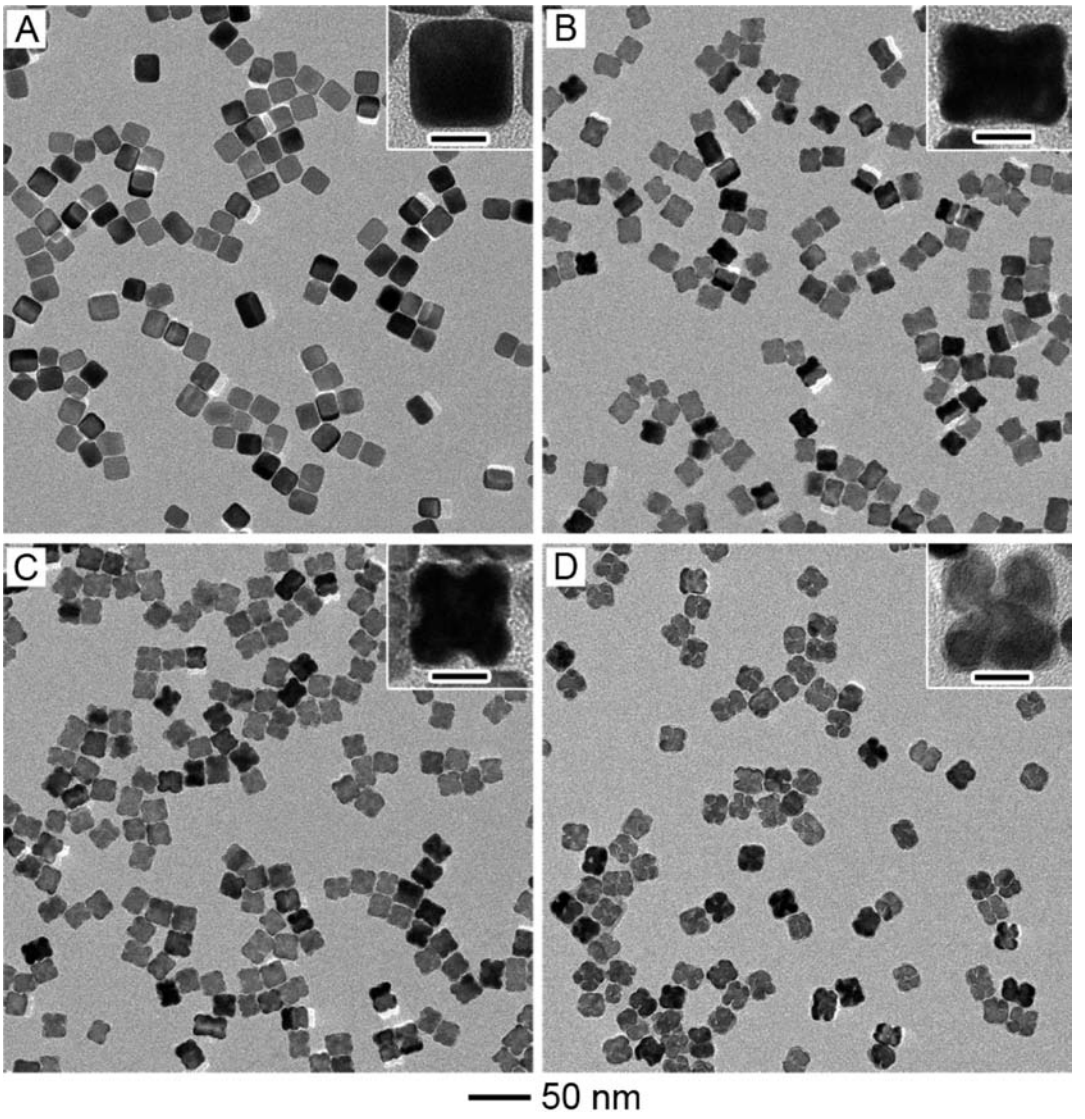

Figure 1. TEM images of Pd−Pt bimetallic nanocrystals prepared via galvanic replacement using the standard procedure, except for different periods of time: (A) 0.5, (B) 4, (C) 9, and (D) 20 h. The insets show TEM images of individual nanocrystals at a higher magnification. The scale bars in the insets are 10 nm.

Morphological, Structural, and Elemental Characterizations. Transmission electron microscopy (TEM) images were taken using a Tecnai G2 Spirit Twin microscope (FEI, Hillsboro, OR) operated at 120 kV. High-resolution TEM (HRTEM), high-angle annular dark-field scanning TEM (HAADF-STEM), and energy dispersive X-ray (EDX) analyses were performed using a JEOL 2100F microscope (JEOL, Tokyo, Japan) operated at 200 kV. Scanning electron microscopy (SEM) images were captured with a Nova NanoSEM 230 field-emission microscope (FEI, Hillsboro, OR) operated at 30 kV. The percentages of Pd and Pt in the samples were determined using inductively coupled plasma mass spectrometry (ICP-MS) (Perkin-Elmer Elan DRC II ICP-MS).

Electrochemical Measurements. The electrochemical measurements were performed at room temperature using a rotating disk electrode (Pine Research Instrumentation, United States) connected to a PARSTAT 283 potentialstat (Princeton Applied Research, United States). A hydrogen electrode (Gaskatel, Germany) was used as the reference. The counter electrode was a Pt mesh (1×1 cm^2) connected to a Pt wire. To prepare the working electrode, 15 μL of an aqueous suspension of the catalyst was transferred to the glassy carbon rotating disk electrode. For all Pd−Pt nanocrystals and Pt/C catalyst, the loading of the catalyst was 3 μg based on the mass of the metal(s). Upon drying under air for 2 h, the electrode was covered with 15 μL Nafion dispersed in water (0.05%). The electrolyte was 0.1 M $HClO_4$ prepared by diluting a commercial solution (70%, ACS reagent grade, T. J. Baker) using Millipore ultrapure water. The cyclic voltammetry curves were recorded at room temperature in an N_2-purged (ultrahigh purity, Airgas) 0.1 M aqueous $HClO_4$ solution at a sweep rate of 50 mV/s. The ORR measurements were performed at a sweep rate of 10 mV/s from 0.05 to 1.1 V at 1600 rpm under continuous O_2 flow. The Kouteck−Levich equation was applied to calculate the kinetic current density, which can be described as[36,37]

$$1/j = 1/j_k + 1/j_d$$

where j is the experimentally measured current, j_d is the diffusion-limiting current, and j_k is the kinetic current. For each catalyst, the kinetic current was normalized to the loading of metals (both Pt and Pd for the

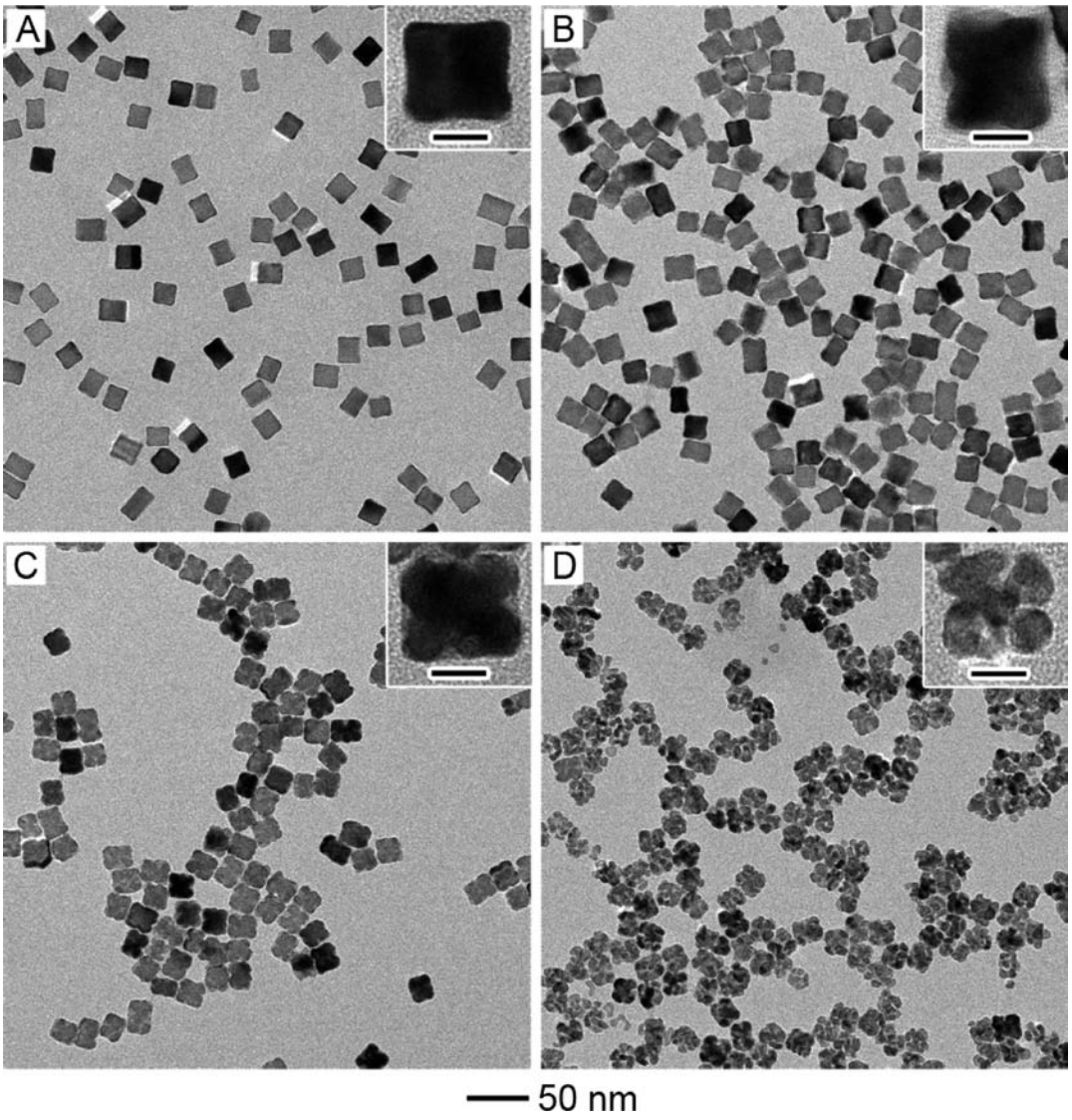

Figure 2. TEM images of Pd−Pt nanocrystals obtained using the standard procedure, except for the addition of different amounts of H_2PtCl_6: (A) 0.5, (B) 1.4, (C) 3.5, and (D) 7.0 mg. The insets show TEM images of individual nanocrystals at a higher magnification. The scale bars in the insets are 10 nm.

Pd−Pt bimetallic nanocrystals or only Pt for Pt/C) in order to obtain mass activity.

RESULTS AND DISCUSSION

Morphological Changes during the Galvanic Replacement Reaction. We monitored the evolution of different morphologies during galvanic replacement by imaging the products obtained at different reaction times. In a set of experiments, Pd nanocubes with an average edge length of 18 nm (Figure S1, Supporting Information) were employed as templates for the galvanic replacement reaction with H_2PtCl_6. A close examination shows that a small portion of the Pd nanocubes were somewhat elongated along one of the axes to form nanobars with aspect-ratios (length to width) slightly larger than one. Since both the nanocubes and nanobars were enclosed by {100} facets, they are collectively called "nanocubes" in the present work for the purpose of simplicity. Figure 1 shows representative TEM images of the Pd−Pt nanocrystals prepared via galvanic replacement using the standard procedure, except the differences in reaction time. In the initial stage of the reaction (t = 0.5 h), the morphology of the Pd templates was essentially maintained. The magnified TEM image (inset of Figure 1A) clearly shows that the nanocube was slightly truncated at corners and bounded by a mix of {100} and {111} facets, which can be attributed to minor oxidative etching caused by the Cl^-/O_2 and Br^-/O_2 pairs.[38,39] After the reaction had proceeded to t = 4 h (Figure 1B), nanocubes with obvious concave faces were obtained due to the galvanic replacement between Pd nanocubes and H_2PtCl_6. The magnified TEM image (inset of Figure 1B) further reveals that each side face of the Pd nanocube was excavated in the center, resulting in the formation of a concave structure. A careful analysis indicated that the truncated corners of the Pd nanocube were sharpened due to the deposition of newly formed Pt atoms at these sites. These images suggest a transition in morphology from Pd nanocubes with relatively sharp corners to slightly truncated Pd nanocubes and then Pd−Pt concave nanocubes. When the reaction further proceeded to t = 9 h (Figure 1C), most of the Pd nanocubes were transformed into Pd−Pt concave nanocubes. We found that a

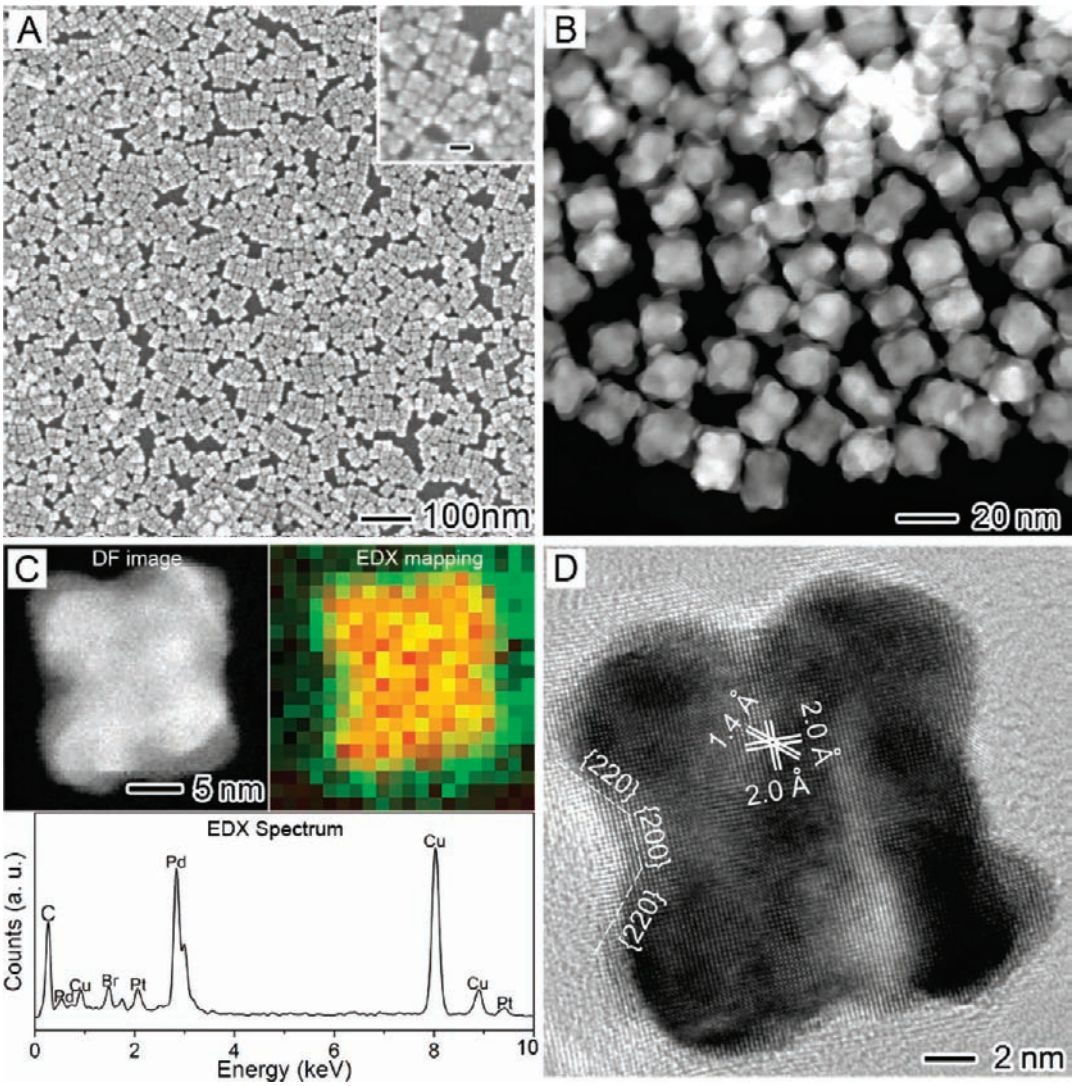

Figure 3. The morphology, structure, and composition of the Pd−Pt concave nanocubes that were prepared using the standard procedure. (A) SEM image, (B) HADDF-STEM image, (C) dark-field TEM and EDX mapping/analysis, and (D) HRTEM image. The inset in (A) shows an SEM image of the nanocrystals at a higher magnification. The scale bars in the inset is 20 nm. The yellow and green colors in (C) correspond to Pd and Pt elements, respectively.

reaction time of 12 h was sufficient to generate Pd−Pt concave nanocubes in high quality. When the reaction time was extended to 20 h (Figure 1D), all the side faces of the Pd nanocubes were found to disappear due to the galvanic replacement. The newly formed Pt atoms preferred to continuously grow these sites close to the corners of a Pd template in order to facilitate the exchange of electrons between Pd and $PtCl_6^{2-}$, eventually leading to the formation of an octapod characterized by slightly elongated arms with enlarged bumps at the tips. Taken together, these results indicate that the galvanic replacement between Pd and $PtCl_6^{2-}$ could readily occur in the presence of Br^-. Furthermore, the oxidation and dissolution of Pd seemed to be preferentially initiated and continued on the {100} side faces.

We could easily control the extent of galvanic replacement between Pd nanocubes and $PtCl_6^{2-}$ ions by varying the amount of H_2PtCl_6. Figure 2 shows typical TEM images of Pd−Pt nanocrystals that were prepared via galvanic replacement with the standard procedure, except the difference in H_2PtCl_6 amount. When reacted with 0.5 mg of H_2PtCl_6 (Figure 2A), the side faces or {100} facets were excavated and tiny tips of Pt started to appear at the corners of each Pd nanocube. When the amount of H_2PtCl_6 was increased to 1.4 mg (Figure 2B), the side faces were further etched due to galvanic replacement, together with deposition of more Pt at the corners of the Pd nanocube, resulting in the formation of Pd−Pt concave nanocubes. After adding 3.5 mg of H_2PtCl_6 (Figure 2C), high-quality Pd−Pt concave nanocubes with an average edge length of 18 nm were obtained. Notably, when the amount of H_2PtCl_6 was further increased to 7.0 mg (Figure 2D), the Pd−Pt concave nanocubes were etched into octapods with large bumps of Pt due to the complete removal of Pd from the {100} faces and extensive lateral deposition of Pt at the corners. This branched structure was also confirmed by SEM imaging (Figure S2, Supporting Information). Taken together, we can conclude that Pd−Pt concave nanocubes with different weight percentages of Pt could be readily obtained by controlling the amount of H_2PtCl_6 dialed into the reaction.

We also used SEM, HRTEM, HAADF-STEM, and EDX to characterize the morphology, structure, and composition of the

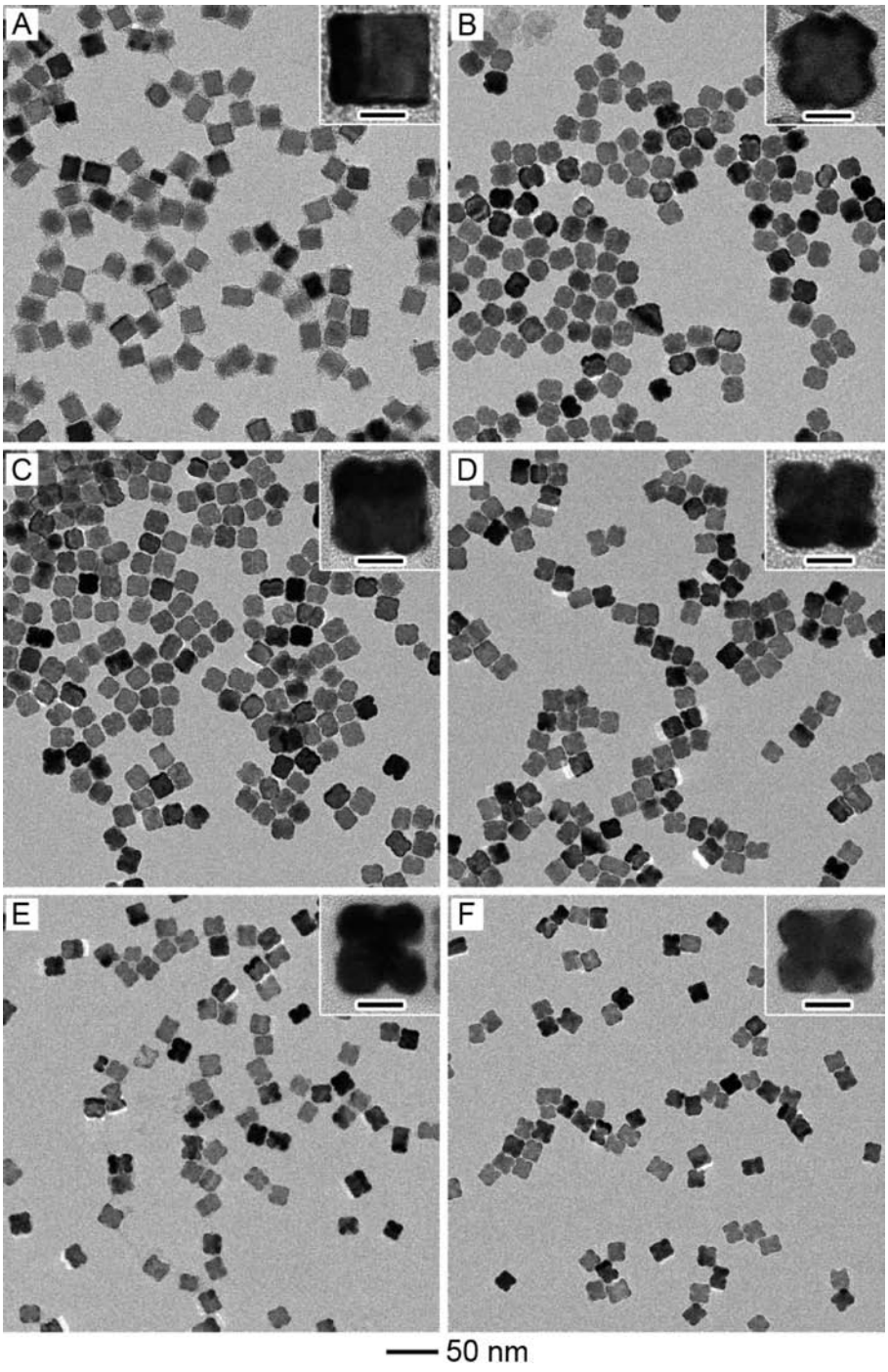

Figure 4. TEM images of Pd−Pt nanocrystals obtained using the standard procedure, except the addition of different amounts of KBr: (A) 0, (B) 8, (C) 20, (D) 60, (E) 150, and (F) 600 mg. The insets show TEM images of individual nanocrystals at a higher magnification. The scale bars in the insets are 10 nm.

Pd−Pt concave nanocubes prepared using the standard procedure. The SEM images in Figure 3A show that most of the Pd−Pt nanocrystals still had a cubic shape, with a size similar to that of the original Pd nanocubes. The side faces of the Pd−Pt nanocubes were concaved due to the galvanic replacement. The concave structure was also supported by HAADF-STEM imaging (Figure 3B). The distribution of Pt and Pd in the concave nanocube was determined using EDX analysis (Figure 3C). As shown by the EDX spectrum, there were five major elements in the sample: Pd, Pt, Br, C, and Cu. Obviously, Pd and Pt came from the Pd−Pt concave nanocubes, while Br, C, and Cu came from the reactant KBr, the PVP coating, and the carbon-coated Cu grid, respectively. The EDX mapping clearly shows a color difference between the interior (mainly Pd, yellow) and the surface (mainly Pt, green), confirming a bimetallic structure. Moreover, most of the Pt was deposited at the corners of the concave nanocube. Figure 3D shows a typical HRTEM image of an individual Pd−Pt concave nanocube along the [100]

dx.doi.org/10.1021/ja201156s |*J. Am. Chem. Soc.* 2011, 133, 6078–6089

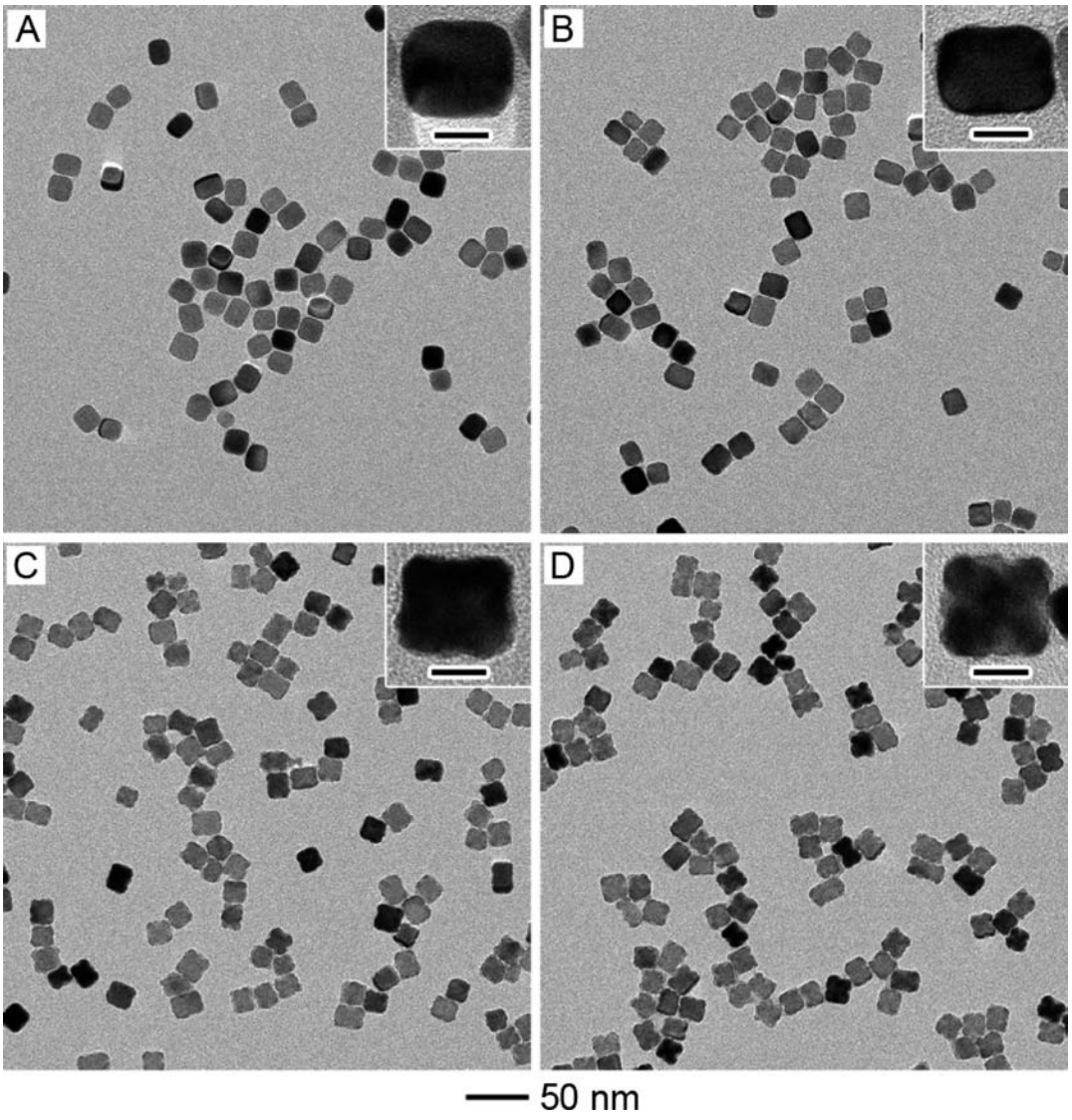

Figure 5. TEM images of Pd−Pt nanocrystals prepared via galvanic replacement using the standard procedure, except the difference in reaction temperature: (A) 50, (B) 60, (C) 70, and (D) 80 °C. The insets show TEM image of individual nanocrystals at a higher magnification. The scale bars in the insets are 10 nm.

zone axis. The HRTEM image clearly shows well-resolved, continuous fringes in the same orientation, indicating that the concave nanocube was a single crystal. We believe that the same crystal structure and negligible lattice mismatch between Pd and Pt (0.77%) were responsible for the formation of a single-crystal, Pd−Pt bimetallic nanostructure during galvanic replacement. The fringes with lattice spacing of 2.0 and 1.4 Å can be indexed to the {200} and {220} planes of a face-centered cubic (*fcc*) lattice, respectively. As a result, the side surface of the concave region is likely bounded by a mix of both {100} and {110} facets.

The Effect of Bromide on the Initiation of Galvanic Replacement. From the viewpoint of potential difference, the galvanic replacement between Pd and $PtCl_6^{2-}$ should be able to occur spontaneously. However, no obvious sign of galvanic replacement between Pd nanocubes and H_2PtCl_6 was observed when they were mixed in an aqueous solution and heated up to 100 °C. In the present work, the galvanic replacement between Pd nanocubes and H_2PtCl_6 seems to be induced and then facilitated by Br^- ions, including the formation of the Pd−Pt concave nanocubes. Figure 4 shows TEM images of Pd−Pt nanocrystals prepared using the standard procedure except for the amount of KBr added into the reaction solution. When no KBr was added (Figure 4A), the side faces of Pd nanocubes were slightly excavated due to oxidation and dissolution of Pd via galvanic replacement reaction with $PtCl_6^{2-}$. In this case, we believe that the small amount of Br^- adsorbed on the {100} side faces of Pd nanocubes during their synthesis was responsible for the galvanic replacement. To support this argument, Pd octahedrons with edge length of 16 nm were also employed as templates for the galvanic replacement reaction in the absence of Br^- (Figure S3, Supporting Information). In this case, no Br^- was used during the synthesis of Pd octahedrons. As a result, no galvanic replacement took place in the case of Pd octahedrons if no additional Br^- ions were added. In this case, $PtCl_6^{2-}$ could be slightly reduced by PVP to generate small Pt nanoparticles as marked by arrows in Figure S3, Supporting Information. As the amount of KBr increased, the resultant Pd−Pt nanocrystals became more concaved on the side faces (Figure 4B−F). We

dx.doi.org/10.1021/ja201156s |*J. Am. Chem. Soc.* 2011, 133, 6078–6089

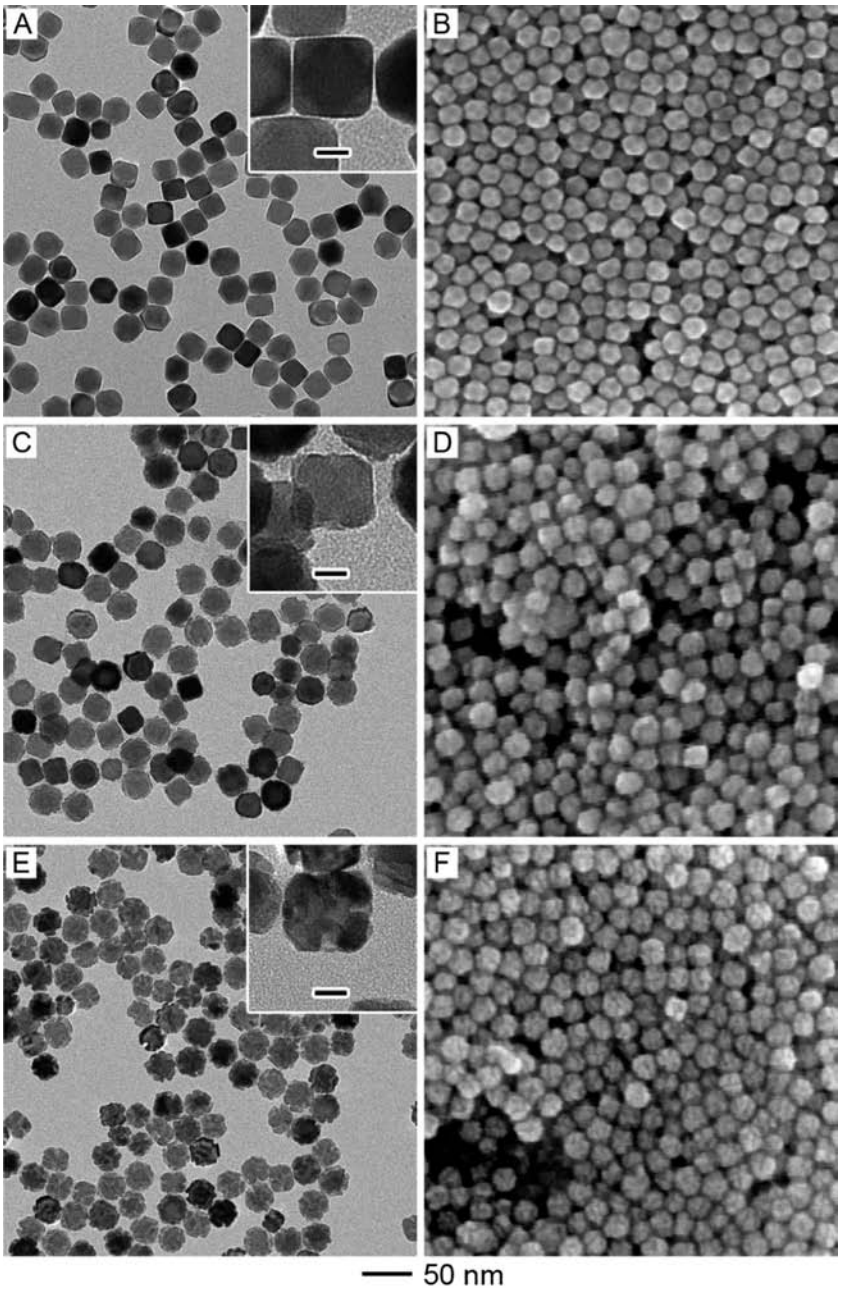

Figure 6. (A) TEM and (B) SEM images of Pd cuboctahedrons with an average edge length of 25 nm. (C and E) TEM and (D and F) SEM images of concave Pd−Pt cuboctahedrons synthesized at 90 °C for 12 h, with 1.4 and 3.5 mg of H_2PtCl_6 being added, respectively. The insets show TEM image of individual nanocrystals at a higher magnification. The scale bars in the insets are 10 nm.

can conclude that Br^- ions played a critical role in both initiating and promoting the galvanic replacement between Pd templates and $PtCl_6^{2-}$.

The Effect of Reaction Temperature. The reaction temperature was also found to play an important role during the formation of Pd−Pt concave nanocubes via galvanic replacement because the rate of galvanic replacement was strongly dependent on this parameter. Figure 5 shows TEM images of Pd−Pt nanocrystals obtained at different reaction temperatures, with all other parameters being the same as in the standard procedure. When the reaction was performed at 50 °C (Figure 5A), the Pd nanocubes were slightly truncated at the corners (which are more active than the side faces) due to oxidative etching by Cl^-/O_2 and Br^-/O_2 pairs. At 60 °C (Figure 5B), atoms started to be removed from the side faces of a Pd nanocube due to galvanic replacement. As the temperature was further increased to 70 °C (Figure 5C), the side faces of a Pd nanocube became more excavated. High-quality Pd−Pt concave nanocubes could not be obtained until the reaction temperature had been increased to at least 80 °C (Figure 5D). We believe that the use of an elevated temperature could speed up the galvanic replacement between Pd nanocubes and $PtCl_6^{2-}$ ions by accelerating the diffusion of $PtCl_6^{2-}$ ions to the Pd nanocubes and that the dissolution of Pd from the surface both are beneficial to the formation of a concave structure.

Galvanic Replacement with Pd Nanocrystals in Different Sizes and Shapes. We also examined Pd nanocrystals with

dx.doi.org/10.1021/ja201156s |*J. Am. Chem. Soc.* 2011, 133, 6078–6089

other different sizes and shapes as the sacrificial templates for the galvanic replacement with $PtCl_6^{2-}$ ions. Figure S4, Supporting Information shows TEM images of Pd nanocubes of 10 and 6 nm in size that were used as the sacrificial templates and their corresponding Pd−Pt concave nanocubes. From the images, it is clear that high-quality Pd−Pt concave nanocubes with roughly the same size as the starting Pd nanocubes were also obtained via the galvanic replacement reaction. Combined with the results obtained from Pd nanocubes of 18 nm in size, we can conclude that the size of Pd−Pt concave nanocubes could be controlled by simply using Pd nanocubes with different sizes as the templates.

Both octahedral and cuboctahedral Pd nanocrystals enclosed by {111} or a mix of {111} and {100} facets were also employed as sacrificial templates for the galvanic replacement in an effort to better understand the selectivity in initiation of the reaction on the {100} facets in the presence of Br^-. Figure 6A and B shows TEM and SEM images of Pd cuboctahedrons of about 25 nm in edge length that served as the sacrificial templates. Careful examination (inset of Figure 6A) indicates that the projected image of a cuboctahedron along the [100] axis consisted of a dark square in the center region corresponding to the {100} facets, four light isoceles triangles corresponding to the {111} facets, and four edges corresponding to the {100} facets. After galvanic replacement reaction with 1.4 mg H_2PtCl_6, the dark square in the center region was slightly thinned, while the four isosceles triangles were thickened, as shown in Figure 6, C and D. The selective etching at the {100} facets due to galvanic replacement and deposition of the formed Pt atoms on the {111} facets was responsible for the changes of contrast in the projected image. As the amount of H_2PtCl_6 was further increased to 3.5 mg, Pd−Pt concave cuboctahedrons were obtained (Figure 6E and F). From these images, the dark square at the center and four edges, corresponding to the {100} facets, were concaved due to selective galvanic replacement, together with the deposition of the formed Pt atoms at the four isosceles triangles corresponding to the {111} facets. These results indicate that the galvanic replacement between Pd nanocrystals and $PtCl_6^{2-}$ ions exhibited a selectivity for the {100} facets of Pd nanocrystals in the presence of Br^-.

The facet selectivity was also observed in the case of Pd octahedrons. Figure S5, Supporting Information shows TEM and SEM images of the Pd octahedrons and their corresponding products obtained with the addition of different amounts of H_2PtCl_6. When Pd octahedrons of 33 nm in size with a smooth surface (Figure S5A and B, Supporting Information) reacted with 1.4 mg H_2PtCl_6, the six sharp corners terminated in the {100} facets were selectively removed, while the eight {111} facets were essentially retained (Figure S5C and D, Supporting Information). Meanwhile, the contrast difference between faces (bright) and edges (dark) indicated that the formed Pt atoms were mainly deposited on the {111} facets, making the surface appear rough under SEM imaging (inset of Figure S5D, Supporting Information). When the amount of H_2PtCl_6 was increased to 3.5 mg (Figure S5E and F, Supporting Information), the {100} facets became increasingly concaved, and the {111} facets were further thickened and roughened due to the continuous deposition of Pt. Obviously, no galvanic replacement reaction was observed on the {111} facets, indicating the selectivity of facet for the Br^--induced galvanic replacement.

Mechanism for the Formation of Pd−Pt Concave Nanocubes. In principle, the galvanic replacement can occur between any two metals with proper difference in redox potentials. Because the reduction potential of $PtCl_6^{2-}$/Pt (0.74 V versus RHE) is more positive than that of $PdCl_4^{2-}$/Pd (0.62 V versus RHE), Pd can be oxidized by $PtCl_6^{2-}$ according to the following equation:

$$2Pd_{(s)} + PtCl_6^{2-}{}_{(aq)} + 2Cl^-{}_{(aq)} \rightarrow Pt_{(s)} + 2PdCl_4^{2-}{}_{(aq)} \quad (1)$$

However, our observations indicate that the galvanic replacement between Pd nanocrystals and $PtCl_6^{2-}$ ions could not occur in the absence of Br^-. From eq 1, we expect that the addition of Cl^- ions could promote galvanic replacement between Pd and $PtCl_6^{2-}$ by shifting the equilibrium to the right side. Figure S6A, Supporting Information, shows TEM image of the product obtained using the standard procedure except that the 300 mg KBr was replaced by 188 mg KCl (to obtain the same molar concentration for Cl^- and Br^-). This image indicates that galvanic replacement did occur due to the presence of a large amount of Cl^-. However, the galvanic replacement induced by Cl^- showed no selectivity toward different facets of the Pd templates, leading to the formation of Pd−Pt nanocrystals with an irregular morphology.

When excess Br^- is used, the galvanic replacement between Pd and $PtCl_6^{2-}$ should occur according to the following equation due to much larger stability constants for $[PdBr_4^{2-}]$ and $[PtBr_6^{2-}]$ relative to $[PdCl_4^{2-}]$ and $[PtCl_6^{2-}]$:[40,41]

$$2Pd_{(s)} + PtBr_6^{2-}{}_{(aq)} + 2Br^-{}_{(aq)} \rightarrow Pt_{(s)} + 2PdBr_4^{2-}(aq) \quad (2)$$

The reduction potential of $PtBr_6^{2-}$/Pt (0.61 V versus RHE) is also more positive than that of $PdBr_4^{2-}$/Pd (0.49 V versus RHE). As a result, Pd can be oxidized by $PtBr_6^{2-}$ according to eq 2, which is expected to be further accelerated in the presence of excess Br^- ions. Due to the selective adsorption of Br^- on the {100} facets of a Pd nanocrystal, the {100} facets (or at least in the vicinity of the surface) of the template is supposed to be populated by the $PtBr_6^{2-}$ complex, which is a key component for both the initiation and continuation of the galvanic replacement reaction. We believe that this chemical difference was responsible for the selective galvanic replacement on the {100} facets of a Pd nanocrystal.

In order to exclude the role of oxidative etching by Br^-/O_2 and Cl^-/O_2 in the formation of concave nanocrystals, KCl instead of H_2PtCl_6 with the same molar concentration of Cl^- was used as a reactant, while keeping other conditions unchanged. Figure S6B, Supporting Information shows TEM image of the product obtained using the standard procedure except that 3.8 mg of KCl instead of 3.5 mg of H_2PtCl_6 was added. In this case, only the sharp corners of the Pd nanocubes were removed due to oxidative etching by Br^-/O_2 and Cl^-/O_2, no sign of galvanic replacement was observed in the absence of H_2PtCl_6. To further identify the role of Br^- ions, $PtCl_4^{2-}$ instead of $PtCl_6^{2-}$ was employed as a precursor, because Br^- ions were supposed not to strongly promote the galvanic reaction between Pd and $PtCl_4^{2-}$ according to the following equation:

$$Pd_{(s)} + PtBr_4^{2-}{}_{(aq)} \rightarrow Pt_{(s)} + PdBr_4^{2-}{}_{(aq)} \quad (3)$$

Because PVP can also reduce $PtBr_4^{2-}$, no PVP was added into this reaction. Figure S7, Supporting Information shows TEM images of the product obtained with $PtCl_4^{2-}$ as a reactant in the absence of PVP. Based on their potential difference ($PtBr_4^{2-}$/Pt = 0.70 V, $PdBr_4^{2-}$/Pd = 0.49 V versus RHE), Pd could be oxidized according to eq 3 in the presence of Br^- ions, and Pd−Pt octapods should be formed when 7.0 mg of K_2PtCl_4 was

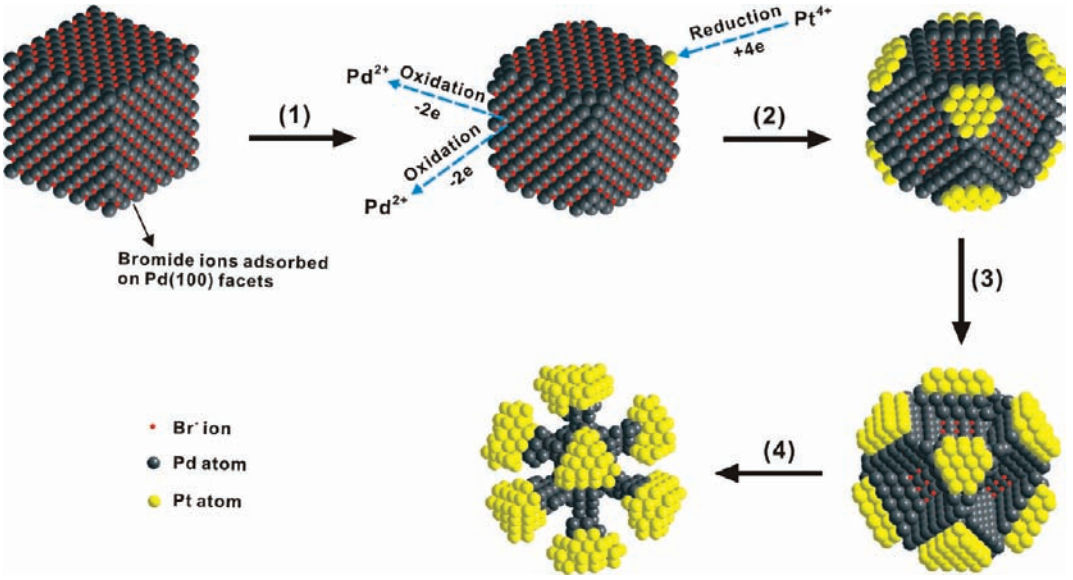

Figure 7. Schematic illustrating a plausible mechanism for the formation of a Pd—Pt concave nanocube through the galvanic replacement between a Pd nanocube and $PtCl_6^{2-}$ ions.

added. However, only the surface of the Pd nanocubes was oxidized by $PtBr_4^{2-}$ due to galvanic replacement. In this case, Br^- ions did not obviously promote the galvanic replacement between Pd and $PtBr_4^{2-}$, which was in agreement with the stoichiometric argument shown in eq 3.

The role of galvanic replacement in the formation of Pd—Pt concave nanocubes was also confirmed by ICP-MS analysis of the molar ratio of Pd^{2+} (in the solution) to Pt (in the concave nanocubes). Obviously, Pd^{2+} could be generated in two different ways: the galvanic replacement between Pd and $PtCl_6^{2-}$ and the oxidative etching of Pd by Br^-/O_2 and Cl^-/O_2. We determined the amount of Pd^{2+} in the solution due to oxidative etching by using KCl instead of H_2PtCl_6 to react with Pd nanocubes. Table S1, Supporting Information, shows the amounts of Pd^{2+} in the solution resulting from oxidative etching in the presence of different amounts of KCl (1.5, 3.1, 3.8, and 7.6 mg) with the same molar concentration of Cl^- as H_2PtCl_6 used in the galvanic replacement experiments (1.4, 2.8, 3.5, and 7.0 mg). It is clear that the Pd^{2+} in the solution obtained through oxidative etching was almost identical in the presence of different amounts of KCl, indicating that the Br^- from 300 mg of KBr was mainly responsible for the oxidative etching. Table S2, Supporting Information, shows the amounts of Pd^{2+} in the solution and Pt in the concave nanocubes resulting from galvanic replacement in the presence of different amounts of H_2PtCl_6. In these cases, we had subtracted the contributions to Pd^{2+} due to oxidative etching. It can be seen that the molar ratio of Pd^{2+}/Pt was approximately 2, in good agreement with eq 2 for the galvanic replacement reaction except for the sample that involved 7.0 mg of H_2PtCl_6. Careful analysis showed that the Pd nanocubes had been etched into Pd—Pt octapods together with a small number of Pt fragments (Figure 2D) in the presence of 7.0 mg of H_2PtCl_6. These Pt fragments with small sizes still exited in the solution after centrifugation, and thus the amount of Pt in the concave nanocubes was underestimated, resulting in a larger than expected molar ratio of Pd^{2+}/Pt. Taken together, the formation of Pd—Pt concave nanocubes can be ascribed to the facet-selective galvanic replacement reaction in the presence of Br^- ions.

Figure 7 illustrates a plausible mechanism responsible for the formation of Pd—Pt concave nanocubes and summarizes the evolution of morphologies during the galvanic replacement reaction. For a nanocrystal with a cubic shape, the reactivity is supposed to decrease in the order of corner, edge, and side face. This difference in reactivity can be further amplified due to the selective adsorption of Br^- on the {100} facets of side faces. As such, in the initial stage, Pd nanocubes were preferentially etched by Br^-/O_2 and Cl^-/O_2 at the corners (the most active sites) in the presence of Br^- and Cl^- (step 1 in Figure 7). After adding a small amount of H_2PtCl_6, the $PtBr_6^{2-}$ complex was formed through replacement of Cl^- in $PtCl_6^{2-}$ by Br^- due to a stronger binding between Br^- and Pt^{4+}.[40] Owing to the selective adsorption of Br^- on the {100} facets, the $PtBr_6^{2-}$ complex was also expected to have a higher concentration in the vicinity of the {100} facets. As a result, Pd atoms on the {100} facets were preferentially oxidized and dissolved by reacting with $PtBr_6^{2-}$. The oxidation of Pd led to the production of electrons, which could quickly migrate to the entire surface of a Pd nanocube. The $PtBr_6^{2-}$ ions in the solution were then reduced to Pt(0) atoms by these electrons and subsequently deposited at the corners of a Pd nanocube (step 2 in Figure 7). This is in contrast to what is involved in the galvanic replacement between truncated Ag nanocubes and $HAuCl_4$, in which the reaction started simultaneously from all corners of a truncated nanocube, while the formed Au atoms were mainly deposited on the side faces due to the strong protection of PVP for Ag {100} facets.[24] As the galvanic reaction proceeded, the Pd {100} facets were gradually removed together with the deposition of more Pt atoms at the corners, resulting in the formation of a Pd—Pt concave nanocube (step 3 in Figure 7). Obviously, the bottom of cavity on the surface of a Pd—Pt concave nanocube was still terminated in Pd atoms, and the newly formed Pt atoms were largely deposited at the corners. Meanwhile, the Pt atoms could also grow laterally, leading to the formation of Pd—Pt octapods with slightly increased arms and large bumps at the tips after complete removal of the Pd {100} facets (step 4 in Figure 7).

dx.doi.org/10.1021/ja201156s |*J. Am. Chem. Soc.* 2011, 133, 6078–6089

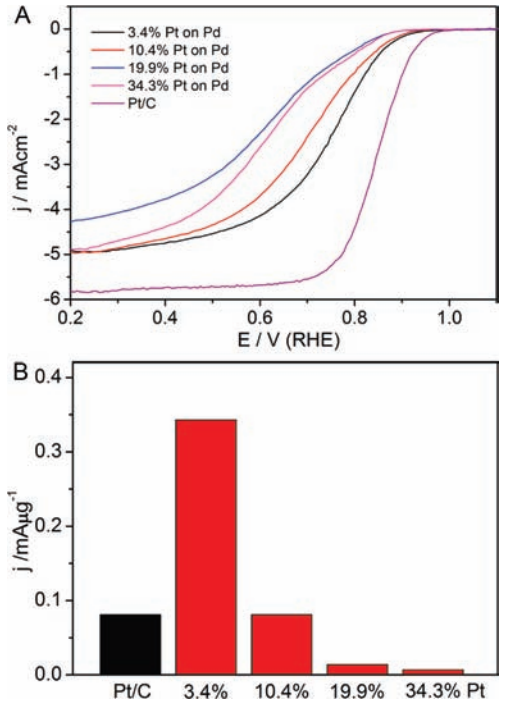

Figure 8. (A) ORR polarization curves for Pt/C and Pd−Pt concave nanocubes (prepared from 18 nm Pd nanocubes) with four different weight percentages for Pt at room temperature in an O_2-saturated 0.1 M $HClO_4$ solution with an equivalent total mass of metals. The data were recorded at a sweep rate of 10 mV/s and a rotation rate of 1600 rpm. For the Pd−Pt concave nanocubes and Pt/C catalysts, the total loading of metals on the RDE was 15.3 $\mu g/cm^2$. The current densities were normalized relative to the geometric area of RDE (0.196 cm^2). (B) The mass activity of these five catalysts normalized by the weight of Pt at 0.9 V versus RHE.

Electrocatalytic Activity toward the ORR. The Pd−Pt concave nanocubes with Pt weight percentages of 3.4, 10.4, 19.9, and 34.4 were obtained via a galvanic replacement reaction with 0.5, 1.4, 3.5, and 7.0 mg of H_2PtCl_6 and then tested as electrocatalysts for the ORR. We benchmarked the electrocatalytic activity of these Pd−Pt nanocrystals against the commercial Pt/C catalyst (E-TEK, 20 wt % of 3.2 nm Pt nanoparticles on Vulcan XC-72 carbon support). Figure S8A, Supporting Information, shows CV curves for these five different catalysts recorded at room temperature in N_2-purged 0.1 M aqueous $HClO_4$ solutions at a sweep rate of 50 mV/s. For all samples, the total loading of metals (both Pd and Pt) on the glassy carbon electrode was 15.3 $\mu g_{metal}/cm^2$. The geometric area of each RDE was 0.196 cm^2. The CV curves exhibited both potential regions associated with H_{upd} adsorption and desorption processes ($H^+ + e^- = H_{upd}$) from 0 to 0.4 V and reversible adsorption of OH_{ad} ($2H_2O = OH_{ad} + H_3O^+ + e^-$) beyond 0.6 V, where H_{upd} and OH_{ad} refer to the underpotentially deposited hydrogen and the adsorbed hydroxyl species, respectively.[42] Due to the intense peak of H_{upd} adsorption and desorption at ~0.05 V originating from the Pd surface uncovered by the Pt shell,[43] the electrochemically active surface area (ECSA) of the Pd−Pt catalyst was underestimated by only measuring the charges collected in the H_{upd} adsorption region from 0.1 to 0.4 V after double-layer correction and assuming a value of 210 $\mu C/cm^2$ for the adsorption of a hydrogen monolayer. The ECSA of the Pt/C catalyst was calculated in the standard region from 0.02 to 0.4 V. The specific ECSA (i.e., ECSA per unit weight of a metal) of the Pd−Pt catalysts with weight percentages of 19.9 and 34.3 was 79.1 and 86.4 m^2/g_{Pt}, respectively, which was comparable to that of the Pt/C catalyst (89.5 m^2/g_{Pt}, see Figure S8B, Supporting Information). In comparison, the Pd−Pt catalysts with low weight percentages (3.4 and 10.4) of Pt exhibited relatively high specific ECSA (185.8 and 125.8 m^2/g_{Pt}).

The ORR measurements were performed in O_2-saturated 0.1 M aqueous $HClO_4$ solutions using a glassy carbon RDE at room temperature at a sweep rate of 10 mV/s and a rotation rate of 1600 rpm. Figure 8A shows the ORR polarization curves for the Pd−Pt concave nanocubes with Pt weight percentages of 3.4, 10.4, 19.9 and 34.4, and Pt/C catalysts. On the basis of an equivalent total mass of Pd and Pt, Pd−Pt concave nanocubes with different percentages of Pt showed relatively lower activities than Pt/C due to the inactive ORR component of Pd. The kinetic current was calculated from the polarization curve by considering the mass-transport correction and normalized with respect to the loading amount of Pt in order to compare the Pt mass activities for different catalysts (Figure 8B). At 0.9 V versus RHE, the Pt mass activities of the Pd−Pt concave nanocubes decreased with weight percentages of Pt, which was in agreement with the trend of specific ECSA. Moreover, the Pd−Pt concave nanocubes with a Pt weight percentage of 3.4 show Pt mass activities four times larger than that of the Pt/C catalyst. Obviously, only those Pt atoms on the surface of a catalyst were directly involved in ORR. Those in the bulk would merely increase the loading of Pt and thus reduce the mass specific activity. For the catalyst with a low weight percentage of Pt, most of the Pt atoms were deposited on the surface of Pd nanocrystals and directly contributed to the ORR activity. In addition, as previously reported by Adzic et al.,[44,45] a Pt monolayer deposited on a Pd surface could have enhanced ORR activity due to an electronic coupling between these two metals. When the amount of Pt atoms exceeded a monolayer, the extra Pt atoms would be deposited on the outer surface with a reduced coupling to the Pd support. As such, the mass specific ORR activity would decrease with increasing Pt weigh percentage. These results suggest that the methodology based on the galvanic replacement between Pd nanocrystals and a Pt salt precursor in the presence of Br^- ions could provide a simple and versatile route to the preparation of highly active ORR electrocatalysts for proton-exchange membrane (PCM) fuel cells.

CONCLUSIONS

We have systematically investigated the galvanic replacement reaction between $PtCl_6^{2-}$ ions and Pd nanocrystals with controllable sizes and well-defined shapes, including cubes, cuboctahedrons, and octahedrons. We have shown that the addition of Br^- ions could promote the galvanic replacement reaction. Specifically, the Br^--induced galvanic replacement reaction showed high selectivity toward the Pd {100} facets, resulting in the formation Pd−Pt concave nanocrystals, for cubes, cuboctahedrons, and octahedrons. It was proposed that the preferential adsorption of Br^- ions on the Pd {100} facets and their strong complexing interaction with Pt^{4+} ions were responsible for the selective galvanic replacement. The Pd−Pt concave nanocubes with a 3.4 wt. % of Pt exhibited the largest specific ECSA and were four times more active for the ORR (on the basis of equivalent Pt mass) than the commercial Pt/C catalyst. This

work not only greatly advances our understanding of the galvanic replacement between Pd nanocrystals and $PtCl_6^{2-}$ ion in the presence of halogen ions (e.g., Br^- and Cl^-) but also provides a facile and versatile approach to the production of Pd−Pt concave nanocrystals with improved electrocatalytic activity for fuel cell applications.

■ ASSOCIATED CONTENT

Supporting Information. TEM images of Pd nanocubes, SEM images of Pd−Pt concave nanocubes, TEM images of Pd octahedrons and their corresponding Pd−Pt nanocrystals prepared in the absence of KBr, TEM images of Pd−Pt concave nanocubes with different sizes, SEM and TEM images of Pd octahedrons and their corresponding Pd−Pt concave structure, TEM images of Pd−Pt nanocrystals synthesized in the presence of KCl, TEM images of Pd−Pt nanocrystals using K_2PtCl_4 as a precursor, ICP-MS data of Pd and Pt, and CV curves and specific ECSA. This material is available free of charge via the Internet at http://pubs.acs.org.

■ AUTHOR INFORMATION

Corresponding Author
xia@biomed.wustl.edu

Author Contributions
‖These authors contributed equally.

■ ACKNOWLEDGMENT

This work was supported in part by a grant from the NSF (DMR-0804088), a DOE subcontract from the University of Delaware (DE-FG02-03 ER15468), and startup funds from Washington University in St. Louis. As a visiting scholar from Zhejiang University, H.Z. was partially supported by the "New Star Program" of Zhejiang University. J.G.W. was also supported by a grant from CNMT (2010K000336) under the 21st Frontier R&D Program of the MEST, Korea. Part of the research was performed at the Nano Research Facility (NRF), a member of the National Nanotechnology Infrastructure Network (NNIN), which is supported by the NSF under award ECS-0335765.

■ REFERENCES

(1) Burda, C.; Chen, X. B.; Narayanan, R.; El-Sayed, M. A. *Chem. Rev.* **2005**, *105*, 1025.
(2) Tian, N.; Zhou, Z. Y.; Sun, S. G.; Ding, Y.; Wang, Z. L. *Science* **2007**, *316*, 732.
(3) Lim, B.; Xia, Y. *Angew. Chem., Int. Ed.* **2011**, *50*, 76.
(4) Tian, N.; Zhou, Z. Y.; Sun, S. G. *J. Phys. Chem. C* **2008**, *112*, 19801.
(5) Camden, J. P.; Dieringer, J. A.; Zhao, J.; Van Duyne, R. P. *Acc. Chem. Res.* **2008**, *41*, 1653.
(6) Ma, Y. Y.; Kuang, Q.; Jiang, Z. Y.; Xie, Z. X.; Huang, R. B.; Zheng, L. S. *Angew. Chem., Int. Ed.* **2008**, *47*, 8901.
(7) Yu, Y.; Zhang, Q. B.; Lu, X. M.; Lee, J. Y. *J. Phys. Chem. C* **2010**, *114*, 11119.
(8) Lu, C. L.; Prasad, K. S.; Wu, H. L.; Ho, J. A. A.; Huang, M. H. *J. Am. Chem. Soc.* **2010**, *132*, 14546.
(9) Xia, Y.; Xiong, Y. J.; Lim, B.; Skrabalak, S. E. *Angew. Chem., Int. Ed.* **2009**, *48*, 60.
(10) Tao, A. R.; Habas, S.; Yang, P. D. *Small* **2008**, *4*, 310.
(11) Lim, B.; Jiang, M. J.; Tao, J.; Camargo, P. H. C.; Zhu, Y. M.; Xia, Y. *Adv. Funct. Mater.* **2009**, *19*, 189.
(12) Herricks, T.; Chen, J. Y.; Xia, Y. *Nano Lett.* **2004**, *4*, 2367.
(13) Au, L.; Lu, X. M.; Xia, Y. *Adv. Mater.* **2008**, *20*, 2517.
(14) Xiong, Y. J.; Wiley, B.; Chen, J. Y.; Li, Z. Y.; Yin, Y. D.; Xia, Y. *Angew. Chem., Int. Ed.* **2005**, *44*, 7913.
(15) Huang, X. Q.; Tang, S. H.; Zhang, H. H.; Zhou, Z. Y.; Zheng, N. F. *J. Am. Chem. Soc.* **2009**, *131*, 13916.
(16) Berkovitch, N.; Ginzburg, P.; Orenstein, M. *Nano Lett.* **2010**, *10*, 1405.
(17) Zhang, J. A.; Langille, M. R.; Personick, M. L.; Zhang, K.; Li, S. Y.; Mirkin, C. A. *J. Am. Chem. Soc.* **2010**, *132*, 14012.
(18) Zhang, H.; Li, W. Y.; Jin, M. S.; Zeng, J.; Yu, T.; Yang, D. R.; Xia, Y. *Nano Lett.* **2011**, *11*, 898.
(19) Yu, T.; Kim, D.; Zhang, H.; Xia, Y. *Angew. Chem., Int. Ed.* **2011**, *50*, 2773.
(20) Sun, Y.; Mayers, B. T.; Xia, Y. *Nano Lett.* **2002**, *2*, 481.
(21) Skrabalak, S. E.; Chen, J. Y.; Sun, Y. G.; Lu, X. M.; Au, L.; Cobley, C. M.; Xia, Y. *Acc. Chem. Res.* **2008**, *41*, 1587.
(22) Seo, D.; Song, H. *J. Am. Chem. Soc.* **2009**, *131*, 18210.
(23) Sun, Y.; Xia, Y. *J. Am. Chem. Soc.* **2004**, *126*, 3892.
(24) Chen, J.; McLellan, J. M.; Siekkinen, A.; Xiong, Y.; Li, Z. Y.; Xia, Y. *J. Am. Chem. Soc.* **2006**, *128*, 14776.
(25) Lu, X.; Tuan, H. Y.; Chen, J.; Li, Z. Y.; Korgel, B. A.; Xia, Y. *J. Am. Chem. Soc.* **2007**, *129*, 1733.
(26) Huang, X.; Zhang, H.; Guo, C.; Zhou, Z.; Zheng, N. *Angew. Chem., Int. Ed.* **2009**, *48*, 4808.
(27) Chen, Z.; Waje, M.; Li, Z.; Yan, Y. *Angew. Chem., Int. Ed.* **2007**, *46*, 4060.
(28) Liang, H. P.; Zhang, H. M.; Hu, J. S.; Guo, Y. G.; Wan, L. J.; Bai, C. L. *Angew. Chem., Int. Ed.* **2004**, *43*, 1540.
(29) Wang, L.; Yamauchi, Y. *J. Am. Chem. Soc.* **2010**, *132*, 13636.
(30) Shao, M. H.; Shoemaker, K.; Peles, A.; Kaneko, K.; Protsailo, L. *J. Am. Chem. Soc.* **2010**, *132*, 9253.
(31) Peng, Z. M.; Yang, H. *J. Am. Chem. Soc.* **2009**, *131*, 7542.
(32) Wang, J. X.; Inada, H.; Wu, L. J.; Zhu, Y. M.; Choi, Y. M.; Liu, P.; Zhou, W. P.; Adzic, R. R. *J. Am. Chem. Soc.* **2009**, *131*, 17298.
(33) Lim, B.; Jiang, M. J.; Camargo, P. H. C.; Cho, E. C.; Tao, J.; Lu, X. M.; Zhu, Y. M.; Xia, Y. *Science* **2009**, *324*, 1302.
(34) Zhang, J.; Vukmirovic, M. B. V.; Xiu, Y.; Mavrikakis, M.; Adzic, R. R. *Angew. Chem., Int. Ed.* **2005**, *44*, 2132.
(35) Jin, M. S.; Liu, H. Y.; Zhang, H.; Xie, Z. X.; Liu, J. Y.; Xia, Y. *Nano Res.* **2011**, *4*, 83.
(36) Bard, A. J.; Faulkner, L. R. *Electrochemical Methods Fundamentals and Application*, 2nd ed.; John Wiley & Sons: New York, 2001.
(37) Schmidt, T. J.; Gasteiger, H. A.; Stäb, G. D.; Urban, P. M.; Kolb, D. M.; Behm, R. J. *J. Electrochem. Soc.* **1998**, *145*, 2354.
(38) Xiong, Y. J.; Chen, J. Y.; Wiley, B.; Xia, Y. *J. Am. Chem. Soc.* **2005**, *127*, 7332.
(39) Xiong, Y. J.; Cai, H. G.; Wiley, B. J.; Wang, J. G.; Kim, M. J.; Xia, Y. *J. Am. Chem. Soc.* **2007**, *129*, 3665.
(40) Srivastava, S. C.; Newman, L. *Inorg. Chem.* **1966**, *5*, 1506.
(41) Feldberg, S.; Klotz, P.; Newman, L. *Inorg. Chem.* **1972**, *11*, 2860.
(42) Gomez, R.; Orts, J. M.; Alvarez-Ruiz, B. L.; Feliu, J. *J. Phys. Chem. B* **2004**, *108*, 228.
(43) Zhang, J.; Huang, M.; Ma, H.; Tian, F.; Pan, W.; Chen, S. *Electrochem. Commun.* **2007**, *9*, 63.
(44) Adzic, R. R.; Zhang, J.; Sasaki, K.; Vukmirovic, M. B.; Shao, M.; Wang, J. X.; Nilekar, A. U.; Mavrikakis, M.; Valerio, J. A.; Uribe, F. *Top. Catal.* **2007**, *46*, 249.
(45) Zhou, W. P.; Yang, X. F.; Vukmirovic, M. B.; Koel, B. E.; Jiao, J.; Peng, G. W.; Mavrikakis, M.; Adzic, R. R. *J. Am. Chem. Soc.* **2009**, *131*, 12755.